Accepted Manuscript online: 2022-08-22 Article published online: 2022-09-20

Development of Rotaxanes as *E*-Field-Sensitive Superstructures in Plasmonic Nano-Antennas

Laurent Jucker[a]
Maximilian Ochs[b]
René Kullock[b]
Yves Aeschi[a]
Bert Hecht[b]
Marcel Mayor[*a,c,d]

[a] Department of Chemistry, University of Basel, St. Johanns-Ring 19, 4056 Basel, Switzerland
[b] Nano-Optics and Biophotonics Group, Experimentelle Physik 5, Universität Würzburg, Am Hubland, 97074 Würzburg, Germany
[c] Institute for Nanotechnology (INT), Karlsruhe Institute of Technology (KIT), P. O. Box 3640, 76021 Karlsruhe, Germany
[d] Lehn Institute of Functional Materials (LIFM), School of Chemistry, Sun Yat-Sen University (SYSU), Guangzhou 510275, P. R. of China
[*] marcel.mayor@unibas.ch

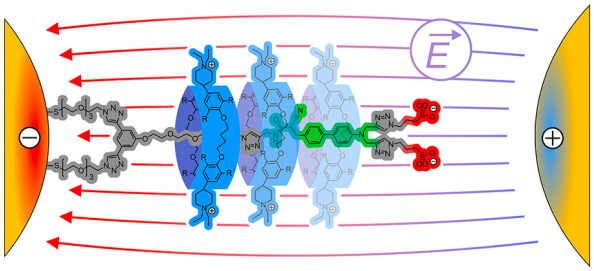

Received: 01.07.2022
Accepted after revision: 14.08.2022
DOI: 10.1055/a-1927-8947; Art ID: OM-2022-07-0016-OA

Abstract We present the concept of electrostatic field-driven supramolecular translation within electrically connected plasmonic nano-antennas. The antenna serves as an anchoring point for the mechanically interlocked molecules, as an electrode for the electrostatic field, and as an amplifier of the antenna-enhanced fluorescence. The synthesis of a push–pull donor–π–acceptor chromophore with optical properties aligned to the antenna resonance is described and its immobilization on the surface is demonstrated. Photoluminescence experiments of the chromophore on a gold nano-antenna are shown, highlighting the molecule–antenna coupling and resulting emission intensity increase. The successful synthesis of an electrostatic field-sensitive [2]rotaxane in water is described and the tightrope walk between functionality and water solubility is illustrated by unsuccessful designs. In solution, an enhanced fluorescence quantum yield is observed for the chromophore comprising the mechanically interlocked [2]rotaxane in water and DMSO compared to the reference rod, ideal for future experiments in plasmonic nano-antennas.

Key words: supramolecular chemistry, molecular switches, opto-electronic materials, nanoelectronics, nanotechnology

Introduction

The inherently independent motion of the individual parts of mechanically interlocked molecules has led to their use as both molecular switches and machines.[1] Rotaxanes in particular are ideal for controlled translational motion of the macrocyclic component (frequently called “shuttling”) along an axis with clear boundaries – the stoppers at either end of the rod.[2,3] This movement is typically induced by external stimuli; common examples include light,[4] acid/base, and redox-driven[5] switching.[1,6]

In solution, the rotaxanes perform the motion along their axis, but due to their random orientation, the movement of the ensemble is isotropic. To achieve anisotropy, rotaxanes and other molecular switches and machines have been immobilized on surfaces and successfully triggered to perform controlled motion.[1,7,8] The immobilization on electrodes provides an ideal platform for electrochemical or electrostatic field-driven switching. While translational motion is frequently achieved on redox-driven rotaxanes, to the best of our knowledge electrostatic fields have mainly been used to study circumrotation of the macrocycle around the rod.[9,10] Solution-based translational motion of DNA- or protein-based strands threaded through nanopores has been achieved with transmembrane electric potentials[11,12] which can be used for sensing DNA polymerase activity[13,14] or protein folding.[15] As demonstrated by these systems, the alignment of the axis along the electric field is an important prerequisite for the electrostatic field-induced translational switching.

Here we propose to profit from the electrostatic field inside the gap of an electrically connected plasmonic nano-antenna to manipulate the translation in a tailor-made rotaxane. While we are currently developing the intended experiment, we report here the optimization of the rotaxane structure together with initial studies in a plasmonic nano-antenna set-up demonstrating the suitability of the structure for the purpose. Figure 1 shows the intended switching experiment and indicates the first prerequisite for meaningful switching inside the antenna gap: site-selectively func-

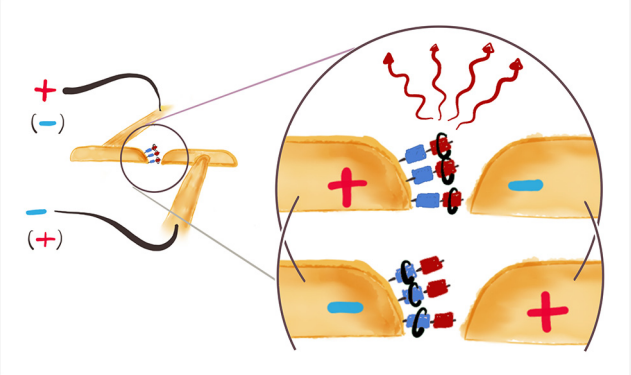

Figure 1 Working principle of an electrostatic field-driven molecular switch based on a [2]rotaxane attached to a plasmonic nano-antenna made of gold. The plasmonic nano-antenna comprises two nanoelectrodes separated by a 30 nm feed gap and electrically connected via two narrow gold wires.

tionalized electrodes. The boundary conditions of the experiment are manifold, ranging from experimental physical challenges over the physical chemistry of the immobilization to aspects that have to be considered in the design of the rotaxane. The most fundamental requirements for the rotaxane are: (1) it must consist of charged subunits to be able to react on the applied electrostatic field. (2) As the translation of the macrocycle along the axis shall be observed optically, one of the stations should be an emitting chromophore, with emission features depending on the presence/absence of the macrocycle. (3) The emission features of the chromophore have to be above 550 nm to avoid the intense inherent emission and interband absorption of gold – the plasmonic nano-antenna material. Furthermore, the chromophore must be sufficiently photostable to allow for the detection of a small ensemble of molecules for a reasonable amount of time. (4) The rotaxane structure must expose anchor groups enabling their immobilization on the gold structure of the optical antenna.

We chose plasmonic nano-antennas as they provide the ideal platform for controlled supramolecular translation and simultaneous readout of the macrocycle's position via antenna-enhanced fluorescence. Their benefits include the following:[16–19] (1) the monocrystalline Au(111) surface is readily functionalized with thiol-functionalized molecules. (2) The nanometer-sized gap allows for strong electrostatic fields at relatively low voltages and hence enables the supramolecular movement of rotaxanes immobilized in the gap region without electrochemical degradation. (3) The geometry of the antenna can be adjusted precisely, thus allowing tuning of the antenna resonance to the chromophore's emission wavelength. (4) Once the resonances are aligned, the feed gap exhibits strong near-field enhancement, which leads to a significant increase in the emission intensity of chromophores close to the antenna gap under saturation conditions. Importantly, the near-field enhancement (and the electrostatic field) decreases outside of the gap, thus the emission signal is dominated by rotaxanes in the gap region.[20,21]

Herein, the synthesis of a push–pull donor–π–acceptor chromophore primed for rotaxane assembly and its coupling to optical nano-antennas are described. Furthermore, the design and synthesis of [2]rotaxanes optimized for electrostatic field-driven switching are reported. As a particular challenge, the merger of the desired functionalities in a compact design with sufficient water solubility enabling rotaxane formation driven by the hydrophobic effect is discussed.

Results and Discussion

The elaborate molecular design of **1a⊂M** (Scheme 1) was devised to comprise all the components required for supramolecular switching in an electrostatic field and its optical ob-

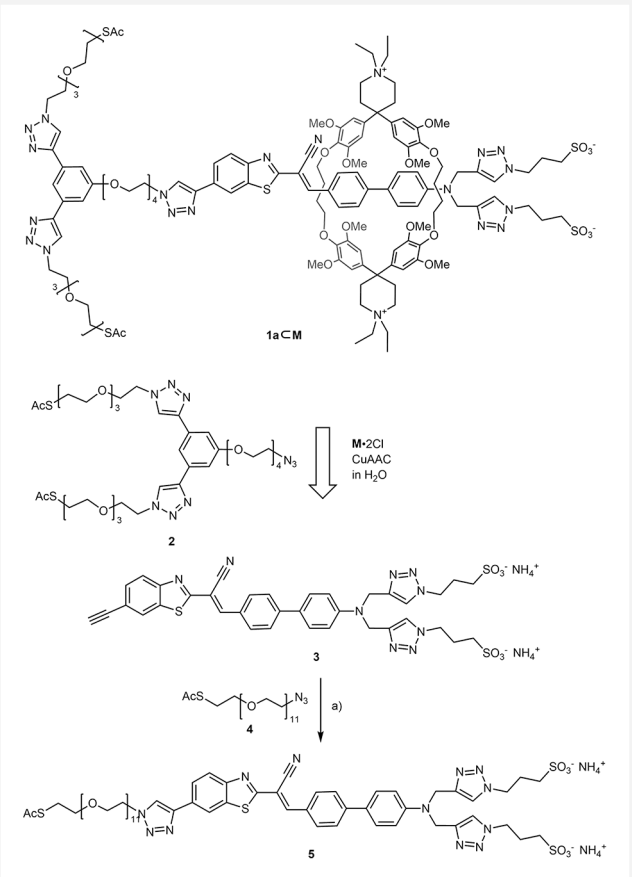

Scheme 1 Design of **1a⊂M** and assembly strategy thereof from stopper **2** and chromophore **3**. Synthesis of **5** via CuAAC of **3** with **4**. Reaction conditions: a) TBTA, $Cu(CH_3CN)_4PF_6$, sodium ascorbate, DMF/H_2O (1:1), r.t., o.n., 35%.

servation. The donor–π–acceptor chromophore serves as both a hydrophobic station for the cyclophane and as a fluorescent readout for the macrocycle's position on the rod. The oligo(ethyleneglycol) (OEG) chain on the rod ensures sufficient space for the cyclophane's translation along the rod axis, while the OEG chains on the stoppers are terminated by masked thiols to anchor the molecule on the gold surface. Both OEG chains further serve to separate the chromophore from the surface to avoid quenching of the chromophore's excited states.[22,23] Stoppers at the ends of the rod mechanically interlock the dicationic macrocycle **M**. We chose the Diederich-type cyclophane **M**[24,25] due to its permanently charged piperidinium groups, the high association constants it exhibits in water, its ability to change emission properties of guests, as well as the ease of analysis by NMR due to its high symmetry and significant changes in chemical shifts upon complexation.[26–30] As additional water-solubilizing groups, anionic sulfonates were considered, pulling the rod towards the cathode and thereby supporting an upright arrangement of the rotaxane immobilized on the anode.

To take advantage of the antenna's near-field enhancement, it is essential for the chromophore to match the antenna resonance, i.e. emitting light in the red spectral region. Simultaneously, the chromophore needs to be sufficiently narrow to fit into the cyclophane's cavity. Accordingly, chromophore **3** was designed to have both a strongly electron-withdrawing group and an electron-donating group bridged by a biphenyl system. Knoevenagel condensation allowed us to combine a terminal alkyne-functionalized benzothiazole and a versatile aldehyde precursor previously synthesized in our group (Scheme S3).[26] The synthesis is described in the Supporting Information. The electron-donating amine on **3** is decorated with two triazol-propylsulfonate groups, which can act as a mechanical stopper and a water-solubilizing group simultaneously. As a result, the chromophore is water soluble and thus suited for rotaxane assembly driven by the hydrophobic effect.[24] This compact design yielded emission maxima above 700 nm in aqueous solution (Figure S8), paving the way for incorporation in plasmonic nano-antennas.

We decided to test the applicability of this chromophore for the purpose of Au(111) surface immobilization and molecule–antenna coupling in the gap of the optical antenna setup. To this end, we attached a thioacetyl-terminated OEG chain (for the synthesis, see Scheme S2) in a copper(I)-catalyzed azide-alkyne 1,3-cycloaddition (CuAAC) "click" reaction to give the extended chromophore **5** (Scheme 1). The OEG chain was envisioned as spacer to the surface and chosen due to its more hydrophilic character compared to typically employed alkyl chains in self-assembled monolayers (SAMs). This allows us to better anticipate potential difficulties in the rotaxane assembly, which will contain OEG chains as linkers as well. The additional 1,2,3-triazol has a small impact on the optical properties, shifting absorption bathochromically and emission hypsochromically, but the emission in the red spectral range is preserved (Figure S8). To deprotect the masked thiol anchoring group and immobilize the molecule on Au(111), **5** is dissolved in methanol and a solution of sodium methoxide (5.4 M in methanol) is added. The gold sample is then immersed in this solution for 20 min, washed with water and dried in a stream of nitrogen gas. We could not observe SAM formation by photoluminescence (PL) when **5** was immobilized without prior deprotection.[31]

The PL measurements of **5** irradiated on the plasmonic nano-antenna demonstrated that the resulting emission is enhanced, polarized, and spectrally shaped by the presence of the optical antenna (Figures 2 and S2).[17,32–34] After chemisorption of **5** on an exemplary antenna (Figure 2a), a hyperspectral PL map is recorded by scanning the region of inter-

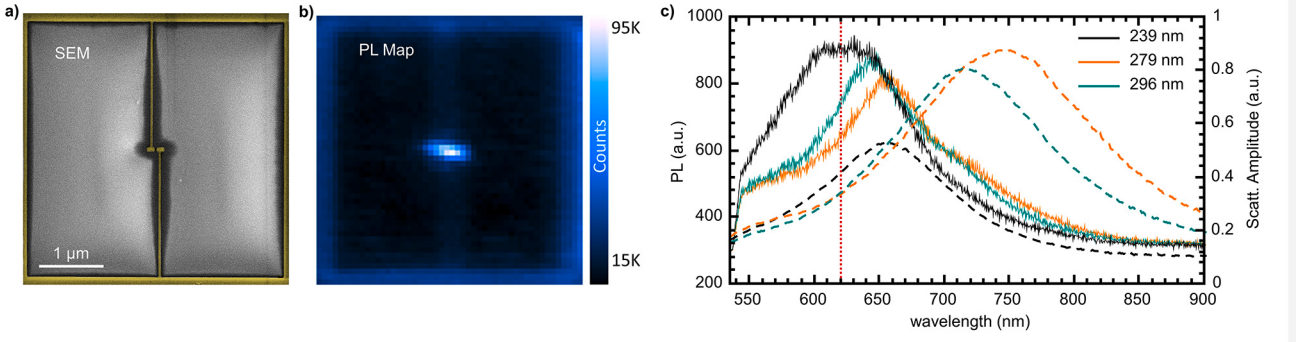

Figure 2 Optical characterization of the molecule–antenna system. **a)** SEM image of an optical antenna with a gap of 30 nm. The plasmonic nano-antenna consists of the two horizontal gold nanorods in the center of the image. The two vertical wires are responsible for providing the electrical contact. **b)** Hyperspectral PL map of the same region as in (a) excited by light of 532 nm wavelength. The light-emitting SAM of **5** covers only the gold surface and its emission is significantly enhanced by the antenna. **c)** PL measurements of nano-antennas of different lengths coated with **5**. The PL of the molecule–antenna system (solid lines) is influenced by the scattering spectrum of the gold nano-antennas (dashed lines), showing the molecule–antenna coupling (see Supporting Information). The emission maximum of **5** on flat gold is shown as a red-dotted line at 620 nm.

est with the excitation laser (Figure 2b). Hardly any emission is detected on glass confirming the surface-selective immobilization of **5** on the Au(111) surface. Furthermore, the local density of states is increased in the vicinity of the optical antenna (i.e., mostly inside the gap and towards the antenna ends), resulting in an increased rate of radiative decay of the molecules compared to the non-radiative decay. Hence, a significantly enhanced emission is observed for molecules on the antenna when compared to the flat Au(111) surface under saturation conditions. The high rate of molecule excitation in the antenna gap causes significant photobleaching within seconds ($t_{1/2}$ = 4.1 s) of irradiation with 50 µW 532 nm light under a stream of nitrogen gas (Figure S1). Nonetheless, the chromophore is sufficiently stable to observe its emission after 30 s of irradiation and is therefore suited for the intended switching experiments.

Due to the shape of the antenna, the enhancement is polarization-dependent and most photons are polarized along the long axis of the antenna (see Supporting Information). The resulting emission peak is closer to the strong resonance of the antenna at 650 nm than the emission polarized along the short axis.

We have repeated these experiments with different antenna lengths to observe the impact of a change in resonance energy (Figure 2c). As expected, the emission enhancement mainly affects transitions in the chromophore close to the resonance energies of the antenna. The maximum of PL emission is shifted bathochromically when the antenna scattering maximum is shifted to lower energies. Moreover, the PL intensity decreases as the resonances of the chromophore and antenna are further detuned.

These experiments not only show the molecule–antenna coupling and associated emission enhancement, polarization, and frequency shift, but also that the chromophore fulfils the stability requirement of the experiment. This axle design thus seems to be ideal for our intent to immobilize rotaxanes on the antenna and observe the translational motion of the macrocycle along the molecular axis optically.

Encouraged by these results, we developed the stopper **2** based on previous designs[29,35] and incorporated an OEG chain with an azide handle for mild rotaxane stoppering via aqueous CuAAC. Furthermore, in analogy to **5**, it comprises masked thiol anchoring groups for its immobilization on a gold surface. The synthesis of **2** is described in the Supporting Information (Scheme S6) and depicted in Scheme 4.

The assembly of mechanically interlocked superstructures like **1a⊂M** based on the precursor **3** turned out to be challenging. While **3** is soluble in water, mixing it with **M**·2Cl leads to immediate precipitation of both components out of D_2O already at concentrations below 0.5 mM. After unsuccessful screening of the complexation conditions and a variety of ineffective derivatization attempts to increase the water solubility of **3**, the assembly strategy was revised fundamentally (Scheme 2a). The new approach is based on

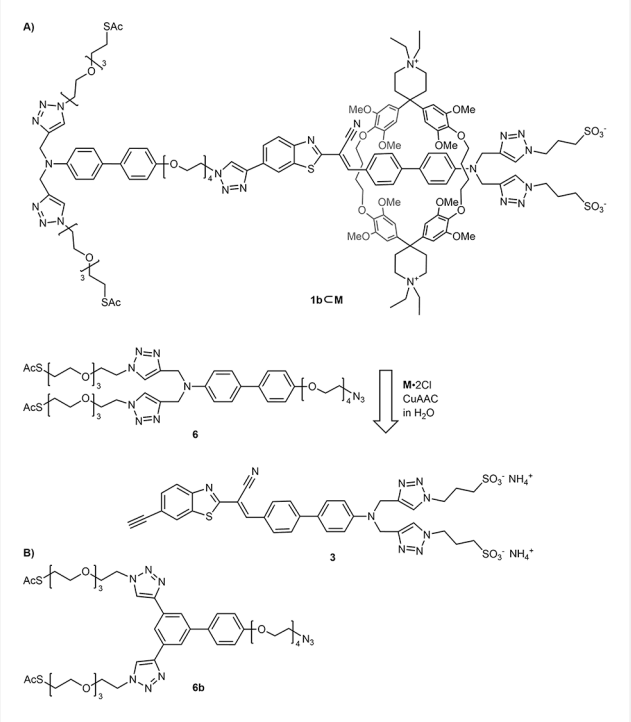

Scheme 2 New rotaxane design inverting the previously employed strategy: **A) 3** acts as a stopper, while **6** serves as a rod for pseudorotaxane formation with **M**·2Cl. Subsequent CuAAC is envisioned to result in mechanically interlocked molecule **1b⊂M. B)** Alternative biphenyl **6b** combining a rod and a stopper.

the biphenyl derivative **6**, with a twofold functionality acting as a terminal stopper and as a guest for the cyclophane host **M**. The plan was to first assemble the pseudorotaxane **6⊂M**, which can subsequently be stoppered with **3** in a CuAAC to form **1b⊂M**. The design of **6** thus comprises a biphenyl hydrophobic station and a doubly substituted amine as stopper, similar to **3**. The synthesis of **6** is described in the Supporting Information (Scheme S4). Despite the OEG chains, the extended stopper **6** was not readily soluble in water. However, to our delight, when heated to 60 °C in the presence of a 2 mM solution of **M**·2Cl in D_2O, the pseudorotaxane **6⊂M** was observed by ^{1}H-NMR spectroscopy after cooling back to room temperature (Scheme S1). Encapsulation of aromatic guests by **M**·2Cl in D_2O is typically associated with strong upfield shifts of the aromatic ^{1}H signals, induced by the aromatic ring current of the cyclophane's walls.[25,36] The observed shielding of the biphenyl protons (up to 2 ppm) confirms the encircling by **M** and the formation of the pseudorotaxane **6⊂M**.

We set out to synthesize **1b⊂M** following this new strategy. First, the pseudorotaxane **6⊂M** was formed by heating **6** in water in the presence of excess **M**·2Cl. Next, $CuSO_4$ and sodium ascorbate were added, followed by chromophore **3** to stopper the pseudorotaxane via CuAAC. While HRMS

(Figure S5) and impure ^{1}H-NMR spectra suggested the formation of **1b⊂M** as an interlocked species, purification attempts revealed that the [2]rotaxane was not a stable mechanically interlocked species in organic solvents like DMSO at room temperature (Figures S6 and S7). Instead an equilibrium between the [2]rotaxane **1b⊂M** and its components **1b** and **M** was observed, resulting in the steady degradation of the isolated [2]rotaxane **1b⊂M**. Intriguingly, we had previously confirmed that the bulk of the triazol-propylsulfonate groups on the chromophore suffice to mechanically interlock a rotaxane.[26] We anticipated **6** to be of similar size but probably underestimated the role of the ionic subunits in the mechanical fixation in solution. However, it appears that the macrocycle can pass the stopper subunit of **6** already at room temperature. We are currently investigating simplified model compounds to rationalize and quantify this observation.

The structure comprising the station for the cyclophane was thus redesigned with a stopper with sufficient steric bulk inspired by **2**. Biphenyl **6b** was supposed to act as a hydrophobic guest for the cyclophane with a pair of attached triazoles exposing OEG chains with terminal anchor groups as stoppers. Its synthesis is presented in the Supporting Information (Scheme S5). In spite of the OEG chains, the compound **6b** turned out to be too insoluble in water to enable the pseudorotaxane formation. Its assembly and properties thus rather display the challenge to find the subtle balance between water solubility and self-assembling features driven by the hydrophobic effect.

Our previously synthesized [2]rotaxane based on chromophore **7** showed increased quantum yields upon encapsulation in both water and DMSO, making it another potential candidate for our endeavor.[26] As a result of the less electron-withdrawing substituent, its absorption and emission are hypsochromically shifted compared to derivatives of **3**. Its optical properties are thus closer to the gold interband absorption, which might increase the challenges faced in the intended experiment. However, with emission signals clearly above 550 nm, it should still be observable individually, and compared to **3**, **7** showed increased water solubility and was shown to have a high association constant with **M**·2Cl in water.[26]

Foregoing the need for a stopper acting as a hydrophobic station, we decided to use our original stopper **2** for our target [2]rotaxane **8⊂M** (Scheme 3). The mechanically interlocked molecule was assembled from **M**·2Cl, **2**, and **7** using classical CuAAC "click" reaction conditions with $CuSO_4$ and sodium ascorbate. All reactants were soluble in water, which allowed us to take full advantage of the hydrophobic effect – the main driving force for the host–guest complexation with **M**.[24] Interestingly, within 2 h at room temperature, the solution had lost nearly all its orange color, and an orange precipitate had formed. This already suggested a significantly decreased water solubility of **8⊂M** and **8** compared to the individual reactants. Purification of the precipitate by re-

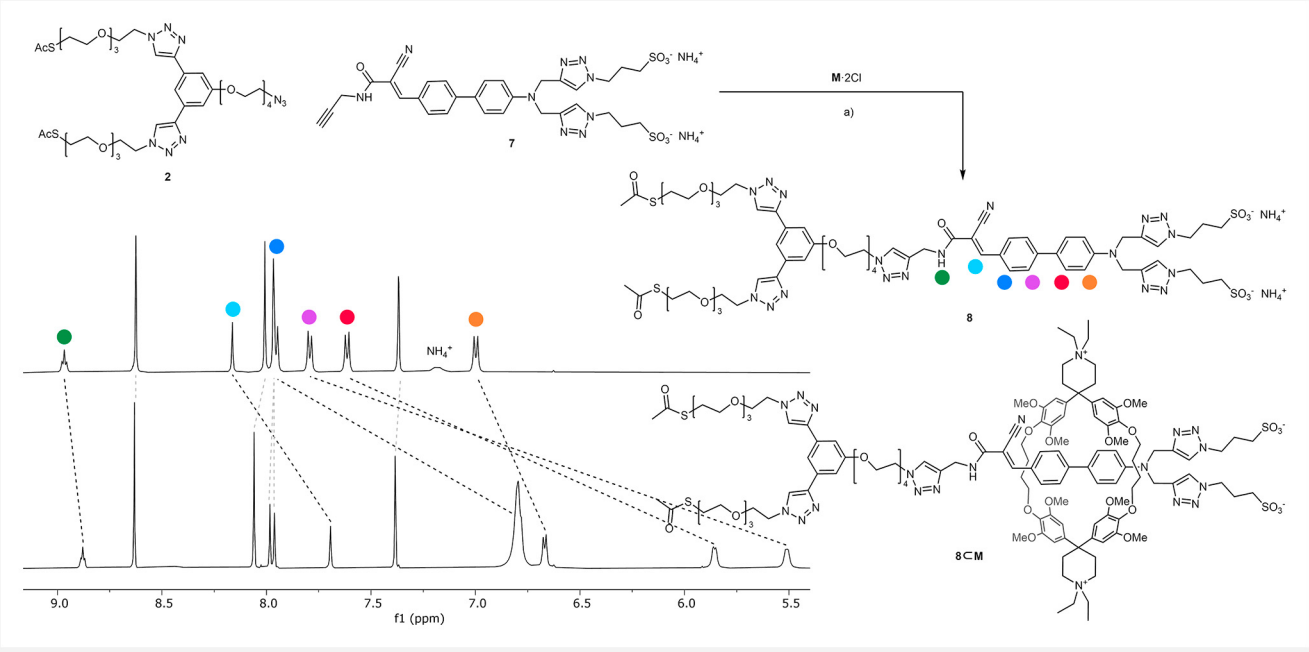

Scheme 3 Synthesis of **8** and **8⊂M** via the CuAAC "click" reaction of stopper **2** and chromophore **7** in aqueous solution. Reaction conditions: a) $CuSO_4 \cdot 5\,H_2O$, sodium ascorbate, r.t., 2 h, 21 % (**8⊂M**), 28 % (**8**). Comparison of an excerpt of the ^{1}H-NMR spectra of **8** (top, 500 MHz) and **8⊂M** (bottom, 600 MHz) in DMSO-*d*6. Colored dots indicate ^{1}H assignments in **8** and dotted lines show the shifts of these signals in **8⊂M**.

versed-phase HPLC on C-18 functionalized silica enabled the separation of [2]rotaxane **8⊂M** from unthreaded rod **8**, and after further purification of **8**, the two products were isolated in 21% and 28% yield, respectively. **8⊂M** and **8** were fully characterized by ^{1}H-, ^{13}C-, and 2D-NMR spectroscopy, along with HRMS. Both the [2]rotaxane and rod showed low solubility in water, but good solubility in DMSO and mixtures of ACN and water. Unlike **1b⊂M, 8⊂M** was found to be a room-temperature-stable mechanically interlocked superstructure, showing neither dissociation in DMSO over time nor during purification by HPLC.

The mechanically interlocked nature of **8⊂M** is made apparent by NOE signals between the rod and the cyclophane (see Supporting Information). Intriguingly, NOEs between the alkyl protons of the triazolpropylsulfonate groups of the stopper and the protons in proximity to the piperidinium of **M** are observed (Figure S11). These signals potentially suggest the attraction of the two oppositely charged water-solubilizing groups. This phenomenon could explain the stability of **8⊂M** compared to **1b⊂M**, where one of the stoppers lacks the anionic moiety. The implication of this attraction on the shuttling behavior in an electrostatic field will be interesting to investigate.

Comparison of the ^{1}H-NMR spectrum of **8⊂M** to that of **8** reveals distinct shielding of the encapsulated protons in the isolated **8⊂M** (Scheme 3). The central protons of the biphenyl system are shifted most significantly compared to **8** with $\Delta\delta$ of 1.8 and 2.3 ppm, indicating their role as the preferred position of the cyclophane. Interestingly, the olefinic and neighboring aromatic protons are shifted more (0.5 and 1.2 ppm, respectively) than the outer biphenyl proton next to the amine (~0.3 ppm). We interpret this as the macrocycle being prevalent on the more electron-deficient part of the chromophore due to its electron-rich aromatic walls. The ^{1}H signal of the amide is only weakly influenced by the cyclophane and the signals belonging to either stopper show negligible changes in chemical shift.

For our intended purpose of electrostatic field-driven switching, we require a significant difference in optical properties of the two states. Thus, the optical properties of the chromophore in the free rod **8** were compared with the ones of the complexed [2]rotaxane **8⊂M**. The absorption maximum of **8⊂M** is only slightly bathochromically shifted compared to **8**, with 422 versus 415 nm in H_2O (Figure S9), and 426 versus 417 nm in DMSO, respectively (Figure 3). On the other hand, the emission is shifted hypsochromically in **8⊂M**, with maxima at 654 and 635 nm in water and DMSO, respectively, compared to 671 and 652 nm for **8**. While the position of the absorption and emission maxima only slightly varied by encapsulating the chromophore in the rotaxane, a significant difference in the emission intensity was observed. Quantification was performed by absolute fluorescence quantum yield measurement in an integrating sphere, corrected for indirect excitation (see Supporting Information). While the encapsulated chromophore in **8⊂M** emitted with an efficiency of 6.5% in water (65.7% in DMSO), the bare chromophore in **8** showed a quantum yield of only 2.2% in water (20.5% in DMSO). We have previously observed similar fluorescence enhancements with mechanically interlocked structures bearing the same chromophore core.[26] These changes in intensity are crucial to observe the electrostatic field-induced switching in an optical antenna gap.

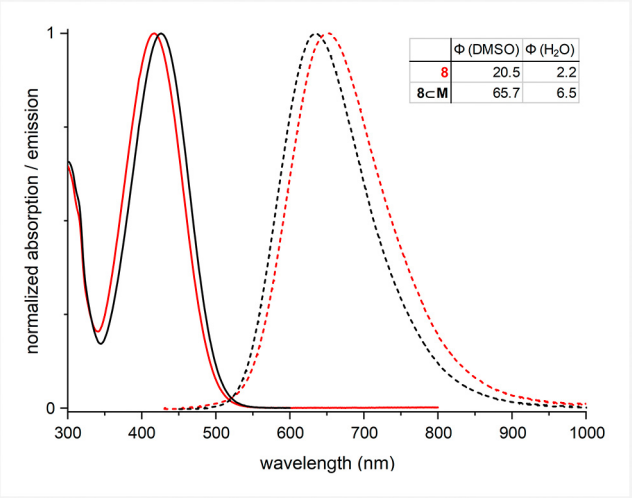

Figure 3 Absorption (solid line) and emission (dashed line) spectra of **8⊂M** (black) and **8** (red) in DMSO solution. The inset table lists the fluorescence quantum yields of both molecules in DMSO and H_2O.

We are delighted to report **8⊂M** as a [2]rotaxane fulfilling the boundary conditions for the intended *E*-field-driven and optically monitored translational switching experiment. Currently we are optimizing the immobilization conditions on Au(111) surfaces with both **8⊂M** and **8**.

Conclusions

The concept of translational motion in a [2]rotaxane within an optical antenna gap by application of an electrostatic field is presented. Initial experiments using a donor–π–acceptor chromophore have proven, besides the robustness of the chromophore, the emission in the vicinity of the antenna to be enhanced, polarized, and influenced in its spectral shape, thereby demonstrating the coupling of the chromophore to the plasmonic nano-antenna. Furthermore, the challenges associated with the aqueous assembly of these complex mechanically interlocked molecules are exemplified by the synthesis of a first [2]rotaxane, which could not be isolated due to spontaneous decomposition of the superstructure in organic solvents. The successful synthesis of a [2]rotaxane as a model compound for the electrostatic field switching inside the gap of a plasmonic nano-antenna is described and

its optical properties are discussed. The fluorescence quantum yield of the mechanically interlocked structure exceeds those of the rod component by about three times – an ideal property to observe positional changes of the cyclophane's position on the axis triggered by the electrostatic field. The site-selective immobilization of these promising model compounds on monocrystalline Au(111) optical antennas is now under investigation and their behavior in electrostatic fields will be studied.

Experimental Section

Experimental procedures and analytical data for building blocks are provided in the Supporting Information. Spectra and NMR assignments are given in the Supporting Information. Macrocycle **M** was synthesized according to the literature-known procedure.[25] Chromophore **7** was previously described by our group.[26] Fabrication of the gold nano-antenna is briefly described in the Supporting Information.
Reagents and solvents were used as received from commercial suppliers (Sigma-Aldrich, Acros, Apollo Scientific, Alfa Aesar, Combi-Blocks, Fluorochem, and TCI Chemicals). Reactions were performed under an argon atmosphere. For column chromatography, Siliaflash P60 (40 – 63 µm) from Silicycle was used with technical-grade solvents (Biosolve). TLC was performed on silica gel 60 F254 aluminium sheets from Merck. ^{1}H NMR, ^{13}C{^{1}H} NMR, and 2D NMR spectra were recorded at 298 K on Bruker Avance III NMR spectrometers equipped with either BBFO, BBI, or BBO probeheads operating at 400 or 500 MHz proton frequencies. For the rotaxane **8⊂M**, NMR spectra were recorded at 298 K on a Bruker Avance III HD NMR spectrometer operating at 600 MHz proton frequency equipped with a QCI-F probehead. The chemical shifts are reported in ppm and referenced to the residual solvent peaks, with coupling constants (J) given in Hz. High-resolution electron spray ionization mass spectrometry (HR-ESI-MS) spectra were recorded on a maXis 4 G instrument from Bruker. UV-Vis absorption spectra were recorded on a Jasco V-770 spectrophotometer equipped with a Peltier-thermostatted cell holder (ETCR-762) set to 25 °C. Emission spectra in solution were recorded on a Jasco FP-8600 spectrofluorometer equipped with a Peltier-thermostatted cell holder (ETC-815) set to 25 °C. Quantum yields were determined on the same spectrofluorometer equipped with a nitrogen-flushed integrating sphere (ILFC-847S). Each measurement for quantum yield determination (blank solvent, direct excitation, indirect excitation) was repeated three times and the average of the three calculated quantum yields was taken.

Synthesis of **5: 3** (97.2 mg, 119 µmol, 1.0 equiv.) and **4** (74.9 mg, 119 µmol, 1.0 equiv.) were dissolved in a mixture of DMF/H_2O (1 : 1, 4 mL) and the resulting solution was degassed with argon for 15 min. TBTA (3.3 mg, 6 µmol, 5 mol %), $Cu(CH_3CN)_4PF_6$ (2.2 mg, 6 µmol, 5 mol%), and sodium ascorbate (1.2 mg, 6 µmol, 5 mol%) were added and the reaction mixture was stirred under argon overnight. The reaction mixture was directly subjected to reverse-phase column chromatography (C18-functionalized silica, 7 : 3 H_2O/ACN buffered with 20 mM NH_4OAc and 0.05% AcOH). The obtained red-orange solid contained acetamide, which was removed by two cycles of sonication in EtOH (20 mL) and subsequent centrifugation. The pure product **5** was obtained as an orange-red solid (60 mg, 35%) after drying in high vacuum.
^{1}H NMR (500 MHz, DMSO-d_6): δ = 8.68 – 8.65 (m, 2 H), 8.39 (s, 1 H), 8.16 – 8.12 (m, 3 H), 8.06 (dd, J = 8.5, 1.7 Hz, 1 H), 8.03 (s, 2 H), 7.87 (d, J = 8.6 Hz, 2 H), 7.68 (d, J = 8.6 Hz, 2 H), 7.05 – 6.92 (m, 8 H) 4.72 (s, 4 H), 4.61 (t, J = 5.1 Hz, 2 H), 4.43 (t, J = 7.1 Hz, 4 H), 3.89 (t, J = 5.2 Hz, 2 H), 3.58 – 3.55 (m, 2 H), 3.53 – 3.43 (m, 46 H), 3.00 (t, J = 6.5 Hz, 2 H), 2.39 (dd, J = 8.2, 6.6 Hz, 4 H), 2.32 (s, 3 H), 2.11 – 2.04 (m, 4 H).
^{13}C NMR (126 MHz, DMSO-d_6): δ = 195.1, 163.8, 152.5, 148.3, 147.7, 145.6, 144.1, 144.0, 135.2, 131.1, 129.7, 128.9, 127.6, 125.9, 125.7, 124.6, 123.4, 123.1, 122.4, 118.5, 116.5, 113.0, 103.3, 69.8, 69.8, 69.7, 69.7, 69.7, 69.6, 69.6, 69.5, 68.9, 68.6, 68.6, 49.8, 48.5, 48.1, 45.6, 37.9, 30.5, 28.3, 26.5.
HRMS-ESI: m/z [M-2NH$_4$ + 5H]$^{3+}$ calcd for ($C_{62}H_{90}N_{14}O_{18}S_4$): 471.8378; found: 471.8378; m/z [M-2NH$_4$ + 4H]$^{2+}$ calcd for ($C_{62}H_{90}N_{14}O_{18}S_4$): 707.2527; found: 707.2541; m/z [2 M-4NH$_4$ + 7H]$^{3+}$ calcd for ($C_{62}H_{90}N_{14}O_{18}S_4$): 942.6679; found: 942.6689; m/z [M-2NH$_4$ + 3H]$^{+}$ calcd for ($C_{62}H_{90}N_{14}O_{18}S_4$): 1413.4982; found: 1413.4986.
UV/Vis (H_2O): λ_{max} = 271, 445 nm.
Fluorescence (H_2O): λ_{max} = 729 nm; Φ_{fl} = 0.6% (H_2O), 16.7% (DMSO).

Synthesis of 3,5-bis((triisopropylsilyl)ethynyl)phenol (**S24**): Reaction conditions were adapted from the literature.[37] 3,5-Dibromophenol (CAS Reg. No. 626 – 41 – 5, 1.26 g, 5.00 mmol, 1.0 equiv.), copper iodide (19 mg, 0.10 mmol, 2 mol%), $Pd(PhCN)_2Cl_2$ (77 mg, 0.20 mmol, 4 mol%), and $HPtBu_3BF_4$ (117 mg, 0.40 mmol, 8 mol%) were dissolved in anhydrous dioxane (15 mL) under an argon atmosphere and stirred at r.t. for 30 min. TIPS-acetylene (2.8 mL, 12.50 mmol, 2.5 equiv.) and $(iPr)_2NH$ (3.5 mL, 25.0 mmol, 5.0 equiv.) in anhydrous dioxane (10 mL) were added to the reaction mixture and the resulting mixture was stirred at r.t. overnight. A solution of HCl (2 M) was added, the product extracted with EtOAc (3×) and the combined organic layers dried with Na_2SO_4, filtered, and the solvent evaporated. The crude product was purified by flash chromatography (gradient cyclohexane to cyclohexane/DCM 70 : 30). The pure product **S24** was obtained as a colorless solid (1.96 g, 86%).
^{1}H NMR (400 MHz, $CDCl_3$): δ = 7.15 (t, J = 1.4 Hz, 1 H), 6.90 (d, J = 1.3 Hz, 2 H), 4.78 (s, 1 H), 1.12 (s, 47 H).

^{13}C NMR (101 MHz, $CDCl_3$): δ = 155.0, 128.3, 125.0, 119.2, 105.8, 91.6, 18.8, 11.4.
HRMS-ESI: *m*/*z* [M + H]$^+$ calcd for ($C_{28}H_{44}OSi_2$): 453.3014; found: 453.3024.

Synthesis of 3,5-diethynylphenol (**S25**): **S24** (1.96 g, 4.31 mmol, 1.0 equiv.) in an argon-flushed flask was dissolved in TBAF solution (1 M in THF, 17.2 mL, 17.2 mmol, 4.0 equiv.) under argon and stirred overnight at room temperature. The solvent was evaporated, the residue was dissolved in TBME and sat. NH_4Cl solution, extracted with TBME (3×) and the extracts washed with sat. NH_4Cl solution, water, and brine. The organic layer was dried with Na_2SO_4, filtered, and the solvent evaporated. Purification by flash chromatography (gradient cyclohexane to DCM) and subsequent trituration of the solid with *n*-pentane gave the pure product **S25** (406 mg, 66%) as a colorless fluffy solid after filtration and drying in high vacuum. The analytical data match the previously reported results.[38]
^{1}H NMR (400 MHz, $CDCl_3$): δ = 7.21 (t, *J* = 1.4 Hz, 1 H), 6.95 (d, *J* = 1.4 Hz, 2 H), 4.91 (s, 1 H), 3.07 (s, 2 H).
^{13}C NMR (101 MHz, $CDCl_3$): δ = 155.2, 128.7, 123.8, 119.7, 82.4, 78.1.
HRMS-ESI: *m*/*z* [M – H]$^-$ calcd for ($C_{10}H_6O$): 141.0346; found: 141.0348.

Synthesis of **S26: S25** (131.9 mg, 0.928 mmol, 1.0 equiv.) and **S13** (540.9 mg, 1.86 mmol, 2.0 equiv.) were dissolved in H_2O/acetone (1 : 4, 2.5 mL). $CuSO_4 \cdot 5\ H_2O$ (23.2 mg, 0.093 mmol, 0.1 equiv.) and sodium ascorbate (37.5 mg, 0.186 mmol, 0.2 equiv.) were added under argon. The reaction mixture was stirred at r.t. for 3.5 h. The mixture was extracted with EtOAc (3×), the extracts washed with brine, dried with Na_2SO_4, filtered, and the solvent evaporated. The crude product was purified by flash chromatography (cyclohexane/acetone 1 : 1) to give the product **S26** as a clear pale-yellow oil (575 mg, 86%).
^{1}H NMR (400 MHz, $CDCl_3$): δ = 8.07 (s, 2 H), 7.86 (t, *J* = 1.4 Hz, 1 H), 7.72 (s, 1 H), 7.45 (d, *J* = 1.5 Hz, 2 H), 4.59 (t, *J* = 4.9 Hz, 4 H), 3.94 – 3.87 (m, 4 H), 3.67 – 3.56 (m, 20 H), 2.71 (dd, *J* = 7.7, 7.0 Hz, 4 H), 1.28 (s, 18 H).
^{13}C NMR (101 MHz, $CDCl_3$): δ = 157.6, 147.5, 132.7, 121.8, 114.9, 112.7, 71.1, 70.7, 70.7, 70.6, 70.3, 69.6, 50.5, 42.3, 31.1, 28.0.
HRMS-ESI: *m*/*z* [M + H]$^+$ calcd for ($C_{34}H_{56}N_6O_7S_2$): 725.3725; found: 725.3722; *m*/*z* [M + Na]$^+$ calcd for ($C_{34}H_{56}N_6O_7S_2$): 747.3544; found: 747.3546.

Synthesis of **S27:** To **S26** (105 mg, 145 µmol, 1.0 equiv.), **S12** (54 mg, 145 µmol, 1.0 equiv.), and K_2CO_3 (40 mg, 290 µmol, 2.0 equiv.) in a round-bottom flask was added DMF (2 mL) under an argon atmosphere. The reaction mixture was heated to 80 °C for 3 d, then allowed to cool to room temperature and extracted with EtOAc (3×). The extracts were dried with Na_2SO_4, filtered, and concentrated under reduced pressure. The crude product was purified by flash chromatography (gradient cyclohexane to cyclohexane/acetone 55 : 45) to give the pure product **S27** as a clear pale-yellow oil (95 mg, 71%).
^{1}H NMR (400 MHz, $CDCl_3$): δ = 8.04 (s, 2 H), 7.87 (t, *J* = 1.4 Hz, 1 H), 7.42 (d, *J* = 1.4 Hz, 2 H), 4.60 (t, *J* = 5.0 Hz, 4 H), 4.27 (t, *J* = 4.8 Hz, 2 H), 3.96 – 3.87 (m, 6 H), 3.77 – 3.53 (m, 30 H), 3.37 (t, *J* = 5.1 Hz, 2 H), 2.69 (t, *J* = 7.3 Hz, 4 H), 1.28 (s, 18 H).
^{13}C NMR (101 MHz, $CDCl_3$): δ = 159.7, 147.4, 132.7, 121.5, 115.7, 111.6, 71.2, 71.0, 70.9, 70.8, 70.8, 70.8, 70.7, 70.7, 70.4, 70.2, 69.9, 69.7, 67.8, 50.8, 50.6, 42.2, 31.1, 28.0.
HRMS-ESI: *m*/*z* [M + H]$^+$ calcd for ($C_{42}H_{71}N_9O_{10}S_2$): 926.4838; found: 926.4831; *m*/*z* [M + Na]$^+$ calcd for ($C_{42}H_{71}N_9O_{10}S_2$): 948.4658; found: 948.4653.

Synthesis of stopper **2:** To a solution of **S27** (83 mg, 89.6 µmol, 1.0 equiv.) in anhydrous ACN (1 mL) under argon was added acetyl chloride (0.68 mL, 9.4 mmol, 105 equiv.), followed by $Bi(OTf)_3$ (60 mg, 89.6 µmol, 1.0 equiv.). The reaction was stirred at r.t. for 5 min, then water was added, and the mixture was extracted with EtOAc (3 µ). The extracts were dried with Na_2SO_4, filtered, and concentrated under reduced pressure. The crude product was purified by reverse-phase HPLC (C-18, ACN/H_2O 65 : 35 + 0.1% HCO_2H) to give the product **2** as a clear colorless oil (40 mg, 50%). A side product was separated by HPLC and its analytical data and presumed structure are given in the Supporting Information.

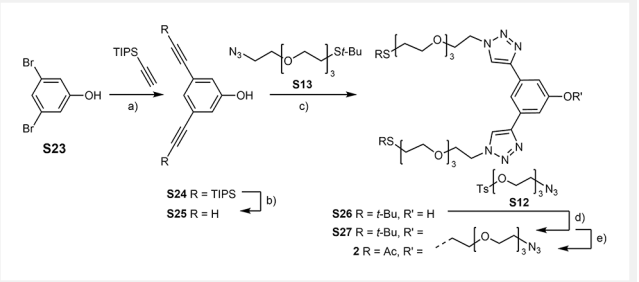

Scheme 4 Synthesis of stopper **2**. Reaction conditions: a) $(i\text{-Pr})_2NH$, CuI,$(PhCN)_2PdCl_2$, $(t\text{-Bu})_3PHBF_4$, dioxane, r.t., o.n., 86%; b) TBAF, THF, r.t., o.n., 66%; c) $CuSO_4 \cdot 5\ H_2O$, sodium ascorbate, acetone/H_2O (4 : 1), r.t., 3.5 h, 86%; d) K_2CO_3, DMF, 80 °C, 5 d, 71%; e) AcCl, $Bi(OTf)_3$, ACN, r.t., 5 min, 50%.

^{1}H NMR (400 MHz, $CDCl_3$): δ = 8.04 (s, 2 H), 7.85 (t, *J* = 1.5 Hz, 1 H), 7.40 (d, *J* = 1.4 Hz, 2 H), 4.58 (t, *J* = 5.0 Hz, 4 H), 4.28 – 4.21 (m, 2 H), 3.93 – 3.86 (m, 6 H), 3.74 – 3.49 (m, 30 H), 3.35 (t, *J* = 5.1 Hz, 2 H), 3.01 (t, *J* = 6.5 Hz, 4 H), 2.28 (s, 6 H).
^{13}C NMR (101 MHz, $CDCl_3$): δ = 195.6, 159.7, 147.2, 132.5, 121.5, 115.7, 111.5, 70.9, 70.8, 70.7, 70.7, 70.7, 70.6, 70.6, 70.3, 70.1, 69.8, 69.7, 69.5, 67.7, 50.7, 50.5, 30.6, 28.8.

HRMS-ESI: *m/z* [M + H]$^+$ calcd for ($C_{38}H_{59}N_9O_{12}S_2$): 838.3797; found: 898.3790; *m/z* [M + Na]$^+$ calcd for ($C_{38}H_{59}N_9O_{12}S_2$): 920.3617; found: 920.3620; *m/z* [M + K]$^+$ calcd for ($C_{38}H_{59}N_9O_{12}S_2$): 936.3356; found: 936.3352.

Synthesis of **8⊂M** and **8:** **7**[26] (8.0 mg, 10.8 µmol, 1.0 equiv.), **M**·2 Cl[25] (12.7 mg, 11.9 µmol, 1.1 equiv.), and **2** (12.0 mg, 13.4 µmol, 1.2 equiv.) were placed in a 25 mL round-bottom flask and flushed with argon. Degassed H_2O (10 mL) was added, the mixture was stirred for 5 min and $CuSO_4 \cdot 5\ H_2O$ (4.5 mg, 18.0 µmol, 1.7 equiv.) and sodium ascorbate (10.0 mg, 49.5 µmol, 4.6 equiv.) were added. The mixture immediately turned turbid and showed formation of an orange precipitate. After stirring at room temperature for 2 h, the precipitate was collected by centrifugation. The crude product was purified by reverse-phase HPLC on C-18 functionalized silica (ACN/H_2O 40 : 60 + 0.5% HCO_2H), allowing the isolation of the pure rotaxane **8⊂M** as an orange-red solid (6.0 mg, 21%). The product proved to be poorly soluble in H_2O or ACN, but well soluble in H_2O/ACN mixtures. The rod **8** eluted with the macrocycle **M** and further purification was necessary. Separation on Sephadex LH-20 (DMF/H_2O 1 : 1, 100 mM NH_4OAc) was unsuccessful. Cyclophane **M** was removed by trituration of the solid with saturated NH_4OAc solution in ACN. The solids were triturated with EtOH to remove excess NH_4OA c. The pure side product **8** was obtained as an orange-red solid (4.9 mg, 28%) after drying in high vacuum.

Analytical data for **8⊂M:**

^{1}H NMR (600 MHz, DMSO-d6): δ = 8.88 (t, *J* = 5.7 Hz, 1 H), 8.63 (s, 2 H), 8.06 (s, 2 H), 7.98 (s, 1 H), 7.96 (t, *J* = 1.5 Hz, 1 H), 7.69 (s, 1 H), 7.38 (d, *J* = 1.4 Hz, 2 H), 6.85 – 6.74 (m, 10 H), 6.67 (d, *J* = 8.4 Hz, 2 H), 5.86 (d, *J* = 8.1 Hz, 2 H), 5.51 (d, *J* = 7.2 Hz, 2 H), 4.67 (s, 4 H), 4.58 (t, *J* = 5.2 Hz, 4 H), 4.54 – 4.48 (m, 8 H), 4.22 (t, *J* = 4.5 Hz, 2 H), 3.88 (t, *J* = 5.2 Hz, 4 H), 3.83 (t, *J* = 5.3 Hz, 2 H), 3.80 (t, *J* = 4.6 Hz, 2 H), 3.72 – 3.19 (m, 92 H, expected: 40 H, overlaps with H_2O, H4), 3.04 – 2.97 (m, 8 H), 2.94 (t, *J* = 6.5 Hz, 4 H), 2.44 (t, *J* = 7.2 Hz, 4 H), 2.29 (s, 6 H), 2.16 – 2.10 (m, 4 H), 1.25 – 1.12 (m, 24 H).

^{13}C NMR (151 MHz, DMSO-d6): δ = 195.1, 161.1, 159.4, 152.9, 150.7, 147.8, 145.9, 144.4, 144.3, 143.4, 134.9, 132.8, 130.1, 127.5, 126.8, 125.3, 124.5, 123.5, 123.2, 122.3, 116.9, 114.4, 112.3, 110.4, 103.1, 101.9, 71.0, 70.0, 69.8, 69.7, 69.7, 69.6, 69.6, 69.5, 69.0, 68.8, 68.8, 68.6, 67.3, 55.6, 55.2, 55.0, 49.7, 49.3, 48.5, 47.9, 45.7, 42.9, 35.4, 30.5, 28.2, 27.7, 26.6, 25.2, 7.0.

HRMS-ESI: *m/z* [M + 3H]$^{3+}$ calcd for ($C_{127}H_{174}N_{20}O_{31}S_4$): 868.7252; found: 868.7268; *m/z* [M + Na]$^+$ calcd for ($C_{127}H_{174}N_{20}O_{31}S_4$): 1302.5841; found: 1302.5861.

UV/Vis: λ_{max} = 422 nm (H_2O), 426 nm (DMSO).

Fluorescence: λ_{max} = 654 nm (H_2O), 635 nm (DMSO); Φ_{fl} = 6.5% (H_2O), 65.7% (DMSO).

Analytical data for **8:**

^{1}H NMR (500 MHz, DMSO-d6) δ 8.97 (t, *J* = 5.7 Hz, 1 H), 8.62 (s, 2 H), 8.16 (s, 1 H), 8.01 (s, 2 H), 7.98 – 7.93 (m, 4 H), 7.79 (d, *J* = 8.2 Hz, 2 H), 7.61 (d, *J* = 8.5 Hz, 2 H), 7.37 (d, *J* = 1.5 Hz, 2 H), 7.18 (s, 1 H, NH_4^+), 7.00 (d, *J* = 8.5 Hz, 2 H), 4.70 (s, 4 H), 4.57 (t, *J* = 5.2 Hz, 4 H), 4.49 (t, *J* = 5.3 Hz, 2 H), 4.47 – 4.40 (m, 6 H), 4.20 (t, *J* = 4.6 Hz, 2 H), 3.88 (t, *J* = 5.2 Hz, 4 H), 3.82 – 3.75 (m, 4 H), 3.61 – 3.43 (m, 22 H), 3.41 (t, *J* = 6.5 Hz, 4 H), 2.94 (t, *J* = 6.4 Hz, 4 H), 2.40 (dd, *J* = 8.3, 6.5 Hz, 4 H), 2.29 (s, 6 H), 2.12 – 2.03 (m, 4 H).

^{13}C NMR (101 MHz, DMSO-d6) δ 195.1, 161.4, 159.3, 150.2, 148.2, 145.9, 144.3, 144.1, 137.7, 134.3, 132.7, 130.9, 129.1, 127.5, 126.0, 125.7, 123.5, 123.1, 122.3, 116.7, 114.3, 113.0, 110.5, 104.0, 70.0, 69.8, 69.6, 69.6, 69.5, 69.5, 68.9, 68.8, 68.7, 68.6, 67.3, 49.7, 49.3, 48.5, 48.0, 45.6, 35.3, 30.5, 28.2, 26.5.

HRMS-ESI: *m/z* [M + 2H + 2Na-2NH$_4$]$^{2+}$ calcd for ($C_{69}H_{98}N_{20}O_{19}S_4$): 825.2727; found: 825.2735; *m/z* [M + 1H + 3Na-2NH$_4$]$^{2+}$ calcd for ($C_{69}H_{98}N_{20}O_{19}S_4$): 836.2636; found: 836.2651; *m/z* [M + 4Na-2NH$_4$]$^{2+}$ calcd for ($C_{69}H_{98}N_{20}O_{19}S_4$): 847.2546; found: 847.2563; *m/z* [M + 2H + 1Na-2NH$_4$]$^+$ calcd for ($C_{69}H_{98}N_{20}O_{19}S_4$): 1627.5561; found: 1627.5535; *m/z* [M + H + 2Na-2NH$_4$]$^+$ calcd for ($C_{69}H_{98}N_{20}O_{19}S_4$): 1649.5381; found: 1649.5352; *m/z* [M + 3Na-2NH$_4$]$^+$ calcd for ($C_{69}H_{98}N_{20}O_{19}S_4$): 1671.5200; found: 1671.5183.

UV/Vis: λ_{max} = 412 nm (H_2O, ε = 18 645 $M^{-1} \cdot cm^{-1}$), 417 nm (DMSO).

Fluorescence: λ_{max} = 671 nm (H_2O), 652 nm (DMSO); Φ_{fl} = 2.2% (H_2O), 20.5% (DMSO).

Funding Information

This project was generously funded by the Volkswagen Foundation (Az. 93 438).

Acknowledgment

We thank Monika Emmerling for preparing gold flakes and substrates.

Supporting Information

Supporting Information for this article is available online at https://doi.org/10.1055/a-1927-8947.

Primary Data

The primary data generated during this study are available at: https://doi.org/10.5281/zenodo.6777943.

Conflict of Interest

The authors declare no conflict of interest.

References

(1) Bruns, C. J.; Stoddart, J. F. *The Nature of the Mechanical Bond: From Molecules to Machines*; Wiley: Hoboken, New Jersey, **2017**.
(2) Kay, E. R.; Leigh, D. A.; Zerbetto, F. *Angew. Chem. Int. Ed.* **2007**, *46*, 72.
(3) Xue, M.; Yang, Y.; Chi, X.; Yan, X.; Huang, F. *Chem. Rev.* **2015**, *115*, 7398.
(4) Yao, B.; Sun, H.; Yang, L.; Wang, S.; Liu, X. *Front. Chem.* **2022**, *9*. doi: 10.3389/fchem.2021.832735
(5) Schröder, H. V.; Schalley, C. A. *Chem. Sci.* **2019**, *10*, 9626.
(6) Tian, H.; Wang, Q.-C. *Chem. Soc. Rev.* **2006**, *35*, 361.
(7) Aprahamian, I. *ACS Cent. Sci.* **2020**, *6*, 347.
(8) Coronado, E.; Gaviña, P.; Tatay, S. *Chem. Soc. Rev.* **2009**, *38*, 1674.
(9) Bermudez, V.; Capron, N.; Gase, T.; Gatti, F. G.; Kajzar, F.; Leigh, D. A.; Zerbetto, F.; Zhang, S. *Proc. SPIE* **2000**, *4106*, 194.
(10) Bermudez, V.; Capron, N.; Gase, T.; Gatti, F. G.; Kajzar, F.; Leigh, D. A.; Zerbetto, F.; Zhang, S. *Nature* **2000**, *406*, 608.
(11) Sánchez-Quesada, J.; Saghatelian, A.; Cheley, S.; Bayley, H.; Ghadiri, M. R. *Angew. Chem. Int. Ed.* **2004**, *43*, 3063.
(12) Biesemans, A.; Soskine, M.; Maglia, G. *Nano Lett.* **2015**, *15*, 6076.
(13) Chu, J.; González-López, M.; Cockroft, S. L.; Amorin, M.; Ghadiri, M. R. *Angew. Chem. Int. Ed.* **2010**, *49*, 10106.
(14) Cockroft, S. L.; Chu, J.; Amorin, M.; Ghadiri, M. R. *J. Am. Chem. Soc.* **2008**, *130*, 818.
(15) Feng, J.; Martin-Baniandres, P.; Booth, M. J.; Veggiani, G.; Howarth, M.; Bayley, H.; Rodriguez-Larrea, D. *Commun. Biol.* **2020**, *3*, 1.
(16) Prangsma, J. C.; Kern, J.; Knapp, A. G.; Grossmann, S.; Emmerling, M.; Kamp, M.; Hecht, B. *Nano Lett.* **2012**, *12*, 3915.
(17) Biagioni, P.; Huang, J.-S.; Hecht, B. *Rep. Prog. Phys.* **2012**, *75*, 024402.
(18) Kern, J.; Kullock, R.; Prangsma, J.; Emmerling, M.; Kamp, M.; Hecht, B. *Nat. Photonics* **2015**, *9*, 582.
(19) Kullock, R.; Ochs, M.; Grimm, P.; Emmerling, M.; Hecht, B. *Nat. Commun.* **2020**, *11*, 115.
(20) Francisco, A. P.; Botequim, D.; Prazeres, D. M. F.; Serra, V. V.; Costa, S. M. B.; Laia, C. A. T.; Paulo, P. M. R. *J. Phys. Chem. Lett.* **2019**, *10*, 1542.
(21) Bardhan, R.; Grady, N. K.; Cole, J. R.; Joshi, A.; Halas, N. J. *ACS Nano* **2009**, *3*, 744.
(22) Anger, P.; Bharadwaj, P.; Novotny, L. *Phys. Rev. Lett.* **2006**, *96*, 113002.
(23) Chi, Y. S.; Byon, H. R.; Lee, B. S.; Kong, B.; Choi, H. C.; Choi, I. S. *Adv. Funct. Mater.* **2008**, *18*, 3395.
(24) Ferguson, S. B.; Seward, E. M.; Diederich, F.; Sanford, E. M.; Chou, A.; Inocencio-Szweda, P.; Knobler, C. B. *J. Org. Chem.* **1988**, *53*, 5593.
(25) Anderson, S.; Aplin, R. T.; Claridge, T. D. W.; Goodson III, T.; Maciel, A. C.; Rumbles, G.; Ryan, J. F.; Anderson, H. L. *J. Chem. Soc., Perkin Trans. 1* **1998**, 2383.
(26) Jucker, L.; Aeschi, Y.; Mayor, M. *Org. Chem. Front.* **2021**, *8*, 4399.
(27) Taylor, P. N.; Hagan, A. J.; Anderson, H. L. *Org. Biomol. Chem.* **2003**, *1*, 3851.
(28) Anderson, S.; Anderson, H. L. *Angew. Chem. Int. Ed. Engl.* **1996**, *35*, 1956.
(29) Aeschi, Y.; Drayss-Orth, S.; Valášek, M.; Raps, F.; Häussinger, D.; Mayor, M. *Eur. J. Org. Chem.* **2017**, *2017*, 4091.
(30) Aeschi, Y.; Jucker, L.; Häussinger, D.; Mayor, M. *Eur. J. Org. Chem.* **2019**, *2019*, 3384.
(31) Béthencourt, M. I.; Srisombat, L.; Chinwangso, P.; Lee, T. R. *Langmuir* **2009**, *25*, 1265.
(32) Zhao, L.; Ming, T.; Chen, H.; Liang, Y.; Wang, J. *Nanoscale* **2011**, *3*, 3849.
(33) Ringler, M.; Schwemer, A.; Wunderlich, M.; Nichtl, A.; Kürzinger, K.; Klar, T. A.; Feldmann, J. *Phys. Rev. Lett.* **2008**, *100*, 203002.
(34) Ming, T.; Zhao, L.; Yang, Z.; Chen, H.; Sun, L.; Wang, J.; Yan, C. *Nano Lett.* **2009**, *9*, 3896.
(35) Aeschi, Y.; Drayss-Orth, S.; Valášek, M.; Häussinge, D.; Mayor, M. *Chem. Eur. J.* **2019**, *25*, 285.
(36) Ferguson, S. B.; Sanford, E. M.; Seward, E. M.; Diederich, F. *J. Am. Chem. Soc.* **1991**, *113*, 5410.
(37) Zhang, Y.; Zhao, C.; Yang, J.; Kapiamba, M.; Haze, O.; Rothberg, L. J.; Ng, M.-K. *J. Org. Chem.* **2006**, *71*, 9475.
(38) Ghosh, K.; Yang, H.-B.; Northrop, B. H.; Lyndon, M. M.; Zheng, Y.-R.; Muddiman, D. C.; Stang, P. J. *J. Am. Chem. Soc.* **2008**, *130*, 5320.